Molecular Catalysis 448 (2018) 63–70

Contents lists available at ScienceDirect

Molecular Catalysis

journal homepage: www.elsevier.com/locate/mcat

Investigation of hollow bimetal oxide nanomaterial and their catalytic activity for selective oxidation of alcohol

Wenbin Gao[a,b], Feng Li[a,b], Hongfei Huo[a,b], Yuanyuan Yang[a,b], Xiang Wang[a,b], Yu Tang[a,b], Pengbo Jiang[a,b], Shuwen Li[a,b], Rong Li[a,b,*]

[a] State Key Laboratory of Applied Organic Chemistry (SKLAOC), College of Chemistry and Chemical Engineering, Lanzhou University, Lanzhou, 730000, PR China
[b] Gansu Provincial Engineering Laboratory for Chemical Catalysis, College of Chemistry and Chemical Engineering, Lanzhou University, Lanzhou, 730000, PR China

ARTICLE INFO

Keywords:
Metal oxide
Hollow nanoparticles
Liquid phase
Kinetic law
Alcohol oxidation

ABSTRACT

The aerobic oxidation procedure utilized sustainable non-noble-metal catalysts has been a long-standing objective in laboratory and industrial research. The synthesized hollow bimetal oxide nanoparticles catalysts (HNPs) as a stable and efficient catalyst, which was applied to the selective oxidation of alcohols with molecular oxygen as oxidant, is reported. The catalytic performance of Co_3O_4/Fe_3O_4@C HNPs was tested via selective aerobic oxidation catalytic reaction of cinnamyl alcohol in the liquid phase. The results prove that the Co_3O_4/Fe_3O_4@C HNPs exhibit ~ 90% yield for alcohol oxidation, which can be conveniently separated and recycled from reaction system by an external magnetism. Forthrmore, the catalyst can be reutilized for at least 5 runs without a distinct activity reduction. A feasible reaction mechnism over the bimetal catalyst for the alcohol oxidation was proposed. The surface effect between metal oxide nanoparticle and carbon support, and relatively high and easy reducibility grant favorable catalytic activity of Co_3O_4/Fe_3O_4@C HNPs. This make the Co_3O_4/Fe_3O_4@C HNPs a very significant catalyst for aerobic catalytic oxidation reaction of alcohols in the liquid phase for industrial manufacture.

1. Introduction

Selective aerobic oxidation of alcohol to the corresponding aldehyde or ketone has turned out to be a very pivotal reaction process in the current of laboratory and chemical industry. Utilization of corresponding products as diverse intermediates for synthesis of key fine chemicals is emerging as a complementary alternative the current energetically inefficient and/or environmentally unfriendly multi-step reactions such as pharmaceuticals, agrochemicals and ploymers [1,2]. Traditionally, many toxic stoichiometric oxidative regents are performed for this oxidation process, which fabricate a lot of waste and pollutants, and are unsanctioned in viewpoint of green and environmental chemistry [3]. From both green and substainable standpoints, there are a strongly moving toward searching and developing the environmental-friendly and green oxidant in this chemosynthesis, such as the air or O_2 being the ideal oxidant from the enviromental point of view [4]. Since these oxidants are readily securable, inexpensive, vast pollution-free natural gas, and water is the main byproduct, that catalytic process is industrially promising alternatives for available alcohol oxidation [5].

In recent years, noble metal nanoparticles have shown a high activity to effect alcohol oxidation using molecular oxygen under moderate temperatures and pressures [1–3]. The heterogeneous precious metal catalysts have been abundantly employed in aerobic oxidation catalysis reaction of alcohols owing to their perfect catalytic property [6], for example, many efficient catalysts based on gold [7,8], palladium [9,10], and platinum [8,11], have been extensively reported and obtained a good result. However, these catalysts possess obvious drawbacks used in practical application, which are expensive cost, limited availability and toxic properties [12,13]. Therefore, considering the drawbacks of noble metal catalysts, it would be still desirable to develop non-noble metal catalysts to affect alcohol oxidation. Moreover, a more significant shortcoming with some of these catalysts in solid-liquid state reaction using molecular oxygen as the oxidant are sensitive for the deactivation of alcohol oxidation due to substrates overoxidation, and a basic condition is needed to activate and enhance catalyst for reaction process [14–16].

Based on the reports of the above, and considered the past study of the non-noble metal and non-noble oxides due to their properties such as non-toxicity, lower cost, fine chemical stability and environmentally

---

[*] Corresponding author at: State Key Laboratory of Applied Organic Chemistry (SKLAOC), College of Chemistry and Chemical Engineering, Lanzhou University, Lanzhou, 730000, PR China.
E-mail address: liyirong@lzu.edu.cn (R. Li).

https://doi.org/10.1016/j.mcat.2018.01.028
Received 28 October 2017; Received in revised form 23 January 2018; Accepted 23 January 2018

friendly [17–22], for example Co_xO_y [23], Fe_xO_y [24], Mn_xO_y [25–28], CeO_x [29], VO_x [22], and many bimetal oxides, including $Co_2Mn_3O_8$ [30], Co-Mn-Al complex oxides [31], Co-Mn oxides [32], Mo-Fe bimetal oxides [33] and others. Meanwhile, cobalt oxide and iron oxide are excellent catalyst for dehydrogenation [24,34,35], CO oxidation [36], CO_2 conversion [37], alcohol oxidation reaction [38], and others. carbon materials due to low density, abundants surface functional grounps, well-diffusion performances and higher specific surface area, are a widely-applied support for plentiful catalytic nanoparticles, and hollow nanoparticles with low density, higher surface-to-volume, their prospective applications in catalysis and others based on nanoscale Kirdendall effect are also proven to be fascinating catalytic support for numerous reaction [39,40]. In addtion, the experiments have demonstrated that the iron oxide and carbon support have special interaction, the negatively charged surface oxygen functional groups of the carbon support serve as strongly active sites for anchoring positively charged Fe^{3+} ions and lead to high dispersion of iron oxide species. These oxygen functional groups also provide a suitable coordinate environment to increase the electron density of iron centres and form efficient active sites for the oxidation of alcohols with molecular oxygen [41].

Herein, considering the previous reported catalysts employed in basic condition and expensive cost limited availability, the catalytic property of the Co_3O_4/Fe_3O_4@C HNPs catalysts was employed in the selective oxidation of alcohol with molecular oxygen in the liquid phase, which shows > 95% alcohol conversion and ~ 90% aldehyde yield without any promoter (eg., NaOH). In addition, the catalyst can be reused after at least 5 runs with a good activity and recycled with external magnetic. This catalyst is a useful and a meaningful candidate for aerobic catalytic oxidation reaction of alcohols in the liquid phase system.

2. Experimental

2.1. Reagents and chemicals

All reagents and chemicals were analytical grade and used as received without any further purification. Ferric (III) nitrate nonahydrate (Fe $(NO_3)_3{\cdot}9H_2O$, 98.5%) was purchased from Chengdu Kelong Chemical Reagents Co., Ltd. Cobalt (II) nitrate hexhydrate (Co $(NO_3)_2{\cdot}6H_2O$, 99.0%) was purchased from Shanghai Zhongqin Chemical Reagents Co., Ltd. Sodium hydroxide (NaOH, 96.0%) was purchased Chemical Reagents Manufacturing Co., Ltd. Sodium oleate ($C_{17}H_{33}COONa$ or NaOA, 99.5%) was purchased from Tianjin Guangfu Chemical Reagents Co., Ltd. Absolute ethanol and hexane was purchased from Lianlong Bohua (Tianjin) Pharmaceutical Chemical Co., Ltd.

2.2. Preparation of the catalyst

In brief, 1 mmol $Fe(NO_3)_3{\cdot}9H_2O$ (0.404 g), 1 mmol $Co(NO_3)_2{\cdot}6H_2O$ (0.291 g) and 5 mmol NaOA (1.522 g) were dissolved in the solution with 10 mL of deionized water, 20 mL absolute ethyl alcohol, and 30 mL of hexane. The mixture solution was heated to 70 °C with magnetic stirring for about 30 min. Then 5 mmol of NaOH (0.200 g) was added to the solution and the mixture solution was stirred for 4 h. After cooled down, the mixture solution was dried at 80 °C for 12 h and a precipitate was obtained. The precipitate mixed with 10 g of Na_2SO_4 was grind to form the homogeneous power, which was heated to 500 °C under nitrogen at heating rate of 10 °C min^{-1} and kept the temperature for 3 h. After cooled down, the black product was washed with deionized water and absolute ethanol, and it was dried at 60 °C for 12 h. Finally the metal nanoparticles (MNPs) loaded on the carbon (MNPs/C) nanocomposites was prepared, which was heated in air 400 °C for 2 h at heating rate of 5 °C min^{-1}, the metal oxide nanoparticles (MONPs) loaded on the carbon (MOHNPs@C) nanocomposites was obtained.

2.3. Catalyst characterization

The crystal phase of the materials was evaluated by X-ray diffractometer (XRD) with a Rigaku D/max-2400 diffractometer using Cu-Ka radiation ($\lambda = 1.5406$ Å). Running condition of XRD and current are 40 kV and 40 mA and the X-ray source in the 2 theta range of 20 − 90°. The full width at half maximum (FWHM) of the XRD line can be used the Schere's formula to estimate the crystallite size from the following equation:

$$D_{XRD} = K\lambda/\beta\cos\theta$$

Where is the observed angular width at half maximum intensity of the peak, K is a dimension less number (equal to 0.89), is the x-ray wavelength (1.5418 Å for Cu Kα) and θ is the diffraction angle. And Inductive coupled plasma optical emission spectrometer (ICP-OES) analysis was carried out with Perkin Elmer (Optima-4300DV) to measure the metal content.

Scanning electron microscopy (SEM) was utilized to observe the image of the samples daubing Carbon double-sided conductive tape with MIRA3 TESCAN. The morphology of the synthesized catalyst was investigated by transmission electron microscopy (TEM) and high-resolution transmission electron microscopy (HR-TEM) with a field emission gun transmission electron microscopy Tecnai G^2Tf^{20} operating at 300 kV and EDX was measured on a Tecnai G^2Tf^{20} microscope. The specimens were dispersed in ethanol and on a holed carbon-coated Cu grid. Nitrogen physisorption isotherms were carried out at −195.8 °C on a static volumetric instrument (TriStar II 3020 V1.04). The specific surface area was calculated by the Brunauer–Emmett–Teller method.

A physical magnetic quality of the sample was researched by a Quantum Design vibrating sample magnetometer (VSM) at room temperature. X-ray photoelectron spectroscopy (XPS) was performed on the PHI-5702 instruments with an Mg anode (Mg Kα hυ = 1253.6 eV) at a base pressure of 5×10^{-8} mbar). The revision of the binding energies (BE) was implemented with the C1 s peak of extraneous C at 284.6 eV.

2.4. Catalytic tests

The reaction was tested in a 25 mL, a three-necked batch reactor with a suitable match reflux condenser, oil bath, and thermocouple at atmospheric pressure. Typically, 4 mmol of substrates, 10 mL of o-xylene and 20 mg of catalyst were mixed with stirring at 393.15 K oxygen (20 mL/min) was continuously brought in bottle and reaction time is 3 h. In addition, the reaction catalyst can be recycled and collected by the external magnetic force, and then it was washed with deionized water and absolute ethanol several times, and following by a heat treatment before next time. Our reaction sample was analyzed by GC–MS (Agilent 6,890N/5,937N).

The catalytic activity was calculated as follows: % conversion = 100 × ($[C_0\text{-}C_1]/[C_0]$), and% Yield = 100 × $[C']/[C_0]$, based on the initial $[C_0]$ and the final $[C_1]$ concentrations of organic substrate and the reaction [C'] concentrations of aldehyde. Turnover Frequency (TOF) = mol number of substrate converted/[moles number of active sites × reaction time].

3. Result and discussion

3.1. Characterizations catalyst

To characterize and prove the morphology of Co_3O_4/Fe_3O_4 HNPs@C, the TEM, HRTEM-mapping and EDX were carried out. Fig. 1a presents a typical TEM image of Co_3O_4/Fe_3O_4 HNPs@C, which clearly exhibits a hollow structure metal oxide nanoparticles of the catalyst, and the sample of Co_3O_4/Fe_3O_4 HNPs@C was successfully obtained. Fig. 1b showed a part of a HNSs with HRTEM and the corresponding morphology sketch. It was observed that the shell of a thin layer of

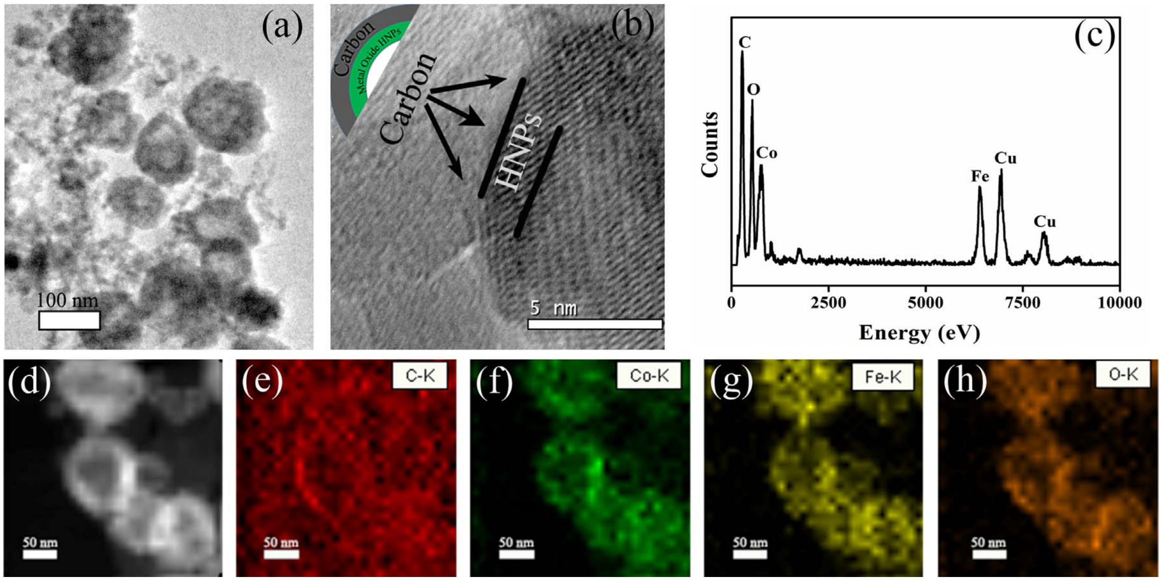

Fig. 1. TEM images (a, b), and EDX (c) and mapping results (d, e, f, g and h) of Co_3O_4/Fe_3O_4@C.

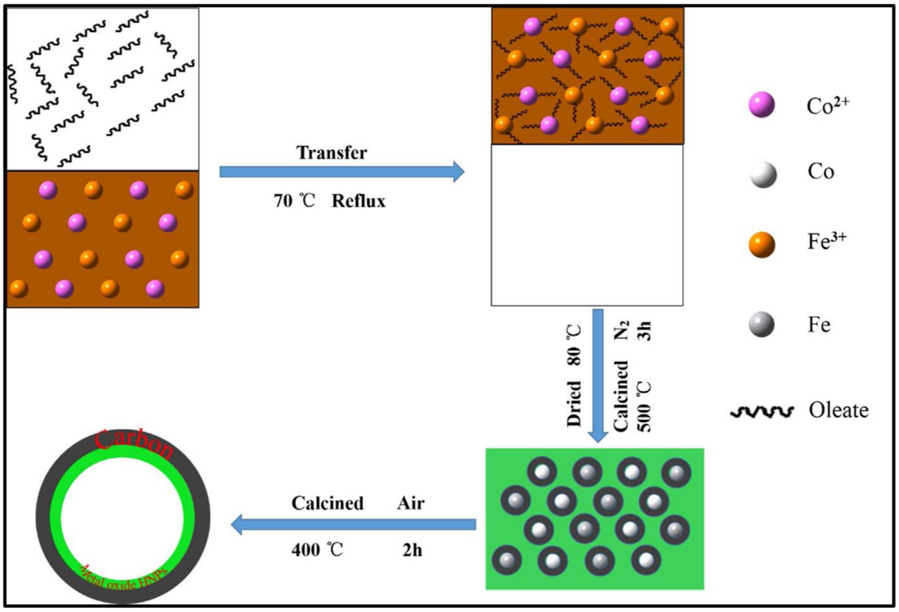

Scheme 1. Schematic caption the synthesis procedure of the material.

Co_3O_4/Fe_3O_4 HNPs. The EDX spectrum of the Co_3O_4/Fe_3O_4 HNPs (Fig. 4c) exhibited the presence of strong signals of C, Cu, Co, Fe and O elements (the scanned region from Fig. 1c) The mapping results of Fig. 1d zone are presented in Fig. 1e–h, in which the distributions of Co, Fe and O elements are the very same. The zone of the distribution of C element was larger than that of Co, Fe, and O, which was consisted with the result that carbon coated on the surface of Co_3O_4/Fe_3O_4 HNSs. Meanwhile, these indicated that Co and Fe elements were evenly dispersed among O element in the inner HNSs layer and carbon was coated on the Co_3O_4/Fe_3O_4 HNSs. In addition, to further insight the morphology of the material, the SEM were presented in Fig. S1. The a-c are CoFe/C and d-f are Co_3O_4/Fe_3O_4@C. Heated under N_2 atmosphere, it is clean that metal NPs/C precuror were obtained and metal nanoparticles were dispered evenly with the carbon nanosheet (see a-c of Fig. S1). Afterwards, the nanocomposites were heated in air, during the procedure, the carbon of the metal NPs/Carbon sheets partly was oxidized and metal NPs transferred to metal oxide HNSs (see d-f of Fig. S1 and TEM) (Scheme 1).

Fig. 2 presents the XRD patterns of the synthesized metal and metal oxide material. The peaks of black line at 2-Theta value of 44.29°, 51.61° and 75.91° in Fig. 2(a) was indicated to cubic Co (JCPDS 00-015-0806). The red line at 2-Theta value of 44.68°, 65.08° and 82.37° and the blue line at 2-Theta value of 37.68°, 42.81°, 43.67° 44.68°, and 49.28° in Fig. 2(a) were displayed to cubic Fe (JCPDS 01-087-0721) and Fe_3C (JCPDS 00-065-0393). The peaks of black line at 2-Theta value of 31.29°, 36.82°, 44.84°, 59.40° and 65.32° in Fig. 2(b) was indicated to cubic Co_3O_4 (JCPDS 00-043-1003). The read line at 2-Theta value of 30.04°, 35.73°, 57.61°, and 62.59° and the blue line at 2-Theta value of 24.20°, 33.31°, 35.65°, 40.94°, 49.51°, 54.10°, and 62.59° in Fig. 2(b) were manifested to cubic Fe_3O_4 (JCPDS 00-082-1533) and rhombohedral Fe_2O_3 (JCPDS 00-033-0664). No other peaks were observed in Fig. 2, which indicated that the metal/C nanocomposites and metal oxide HNSs@C of corresponding phase were synthesized. The the average particles of Fe_3O_4 Fe_2O_3@C, Co_3O_4@C and Fe_3O_4/Co_3O_4@C, were 19.4 nm, 29.3 nm and 20.4 nm in Table 1

The specific surface area and pore size distribution of the porous carbon material structure were certified via N_2 adsorption-desorption analysis. As shown in Fig. 3, the results manifest that the adsorption-

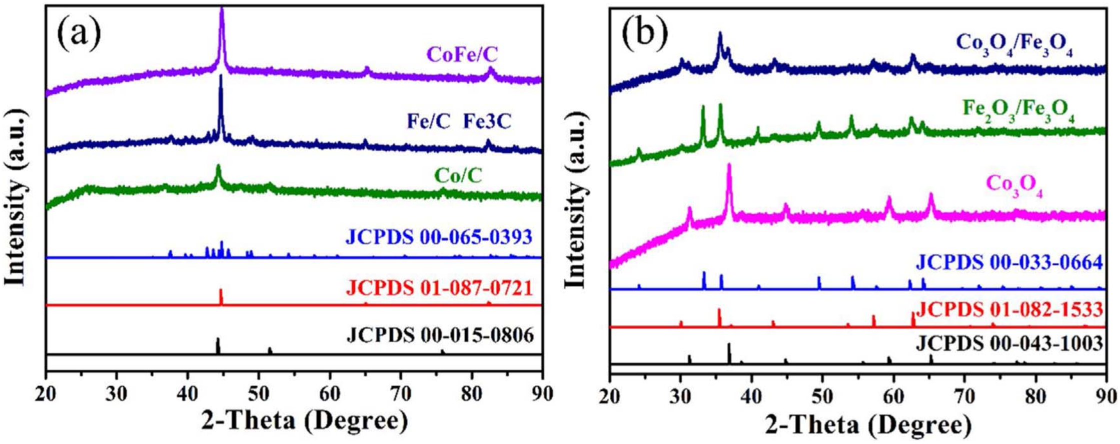

Fig. 2. XRD patterns of (a) MNPs/C; (b) MOHNPs@C.

Table 1
The summary of parameters of the catalyst.

Sample	Surface area (m^2/g)	Pore volume[a] (cm^3/g)	Average pore width[b](nm)	Particle size[c](nm)	E_a kJ/mol	ΔH kJ/mol
Fe Fe_3C/C	141	0.24	7.99	36.2		
Co/C	239	0.27	6.61	22.0		
FeCo/C	332	0.34	5.89	15.1		
Fe_3O_4/Fe_2O_3@C	33	0.16	18.66	19.4	30.0	12.6
Co_3O_4@C	13	0.06	23.25	27.2	27.3	8.9
Co_3O_4/Fe_3O_4@C	28	0.15	26.83	10.4	20.4	4.6

[a] Pore volume is the total pore volume.

[b] Average pore width is the desorption average pore width.

[c] Particle size calculated by the Schere's formula of XRD.

desorption isotherm of the prepared material was a typical type IV isotherm (according to the IUPAC classification) with a hysteresis loop at relatively high P/P_0, indicating the presence of mesoporous morphology of the carbon support. It is clearly that the metal-based materials have higher surface area than metal oxide-based material, which can be attribute to change of pore structure. The result was presented in Table 1.

To gain further insight into the catalyst stucture, XPS characterization was performed to investigate the chemical elements valence states of Co, Fe and O on the surface of Co_3O_4/Fe_3O_4@C. The results were shown in Fig. 4. The Co 2p is spilt into Co $2p_{1/2}$ and Co $2p_{3/2}$, the peak of Co^{3+} located at 779.9 eV and Co^{2+} located at 781.5 eV can be clearly seen from Fig. 4a, which are corresponded with the single Co_3O_4 [38,42]. The two peaks position O 1 s (Fig. 4b) were found to be located at 529–530 eV, which is well-defined in the Co_3O_4 [42], the other two peaks values located at ∼531 eV, and ∼532 eV, can be appointed to carbonyl and carboxylic groups on the carbon surface [38]. And also, Fig. 4c present Fe 2p pattern. The levels of Fe $2p_{3/2}$ and Fe $2p_{1/2}$ are 710.3 eV and 724 eV for Fe^{2+}, and 711.7 eV and 724.8 eV for Fe^{3+}, which are corresponded with that observed from single Fe_3O_4 [43,44]. The O 1 s XPS spectrum on the basis of binding energy of O 1 s has been reported in the literature [24,43].

3.2. Catalysts performance

Table 2 presents the catalytic activity of the different Cobalt and iron-base catalysts. The obvious difference in the catalytic performance of metal-based catalysts and metal oxide-based catalysts can be ascribed to the higher catalytic reaction activity of metal oxide catalysts compared to metal-base catalysts. Also, we study the molar ratio of the range from 3:1, 1:1 and 1:3 of Fe:Co, it was found that Co_3O_4/Fe_3O_4@C with molar ratio of the 1:1 of Fe:Co can obtain ∼90% yield of cinnamyl aldehyde, which is attributed that the more amount of Fe can probably form Fe_2O_3, and the less amount of Fe make the active conment reduce. The result proves that the oxidation procedure is structure sensitive for cobalt oxide and iron oxide, which were demonstrated by dynamic experiment calculated with different global kinetic constant (k_c), adsorption equilibrium constant (K_{ads}) as shown in Table S1, activation energy (E_{act}), and adsorption heat (ΔQ) as shown in Table 1, due to their specific stable surface oxygen vacancies [23,24], favorable

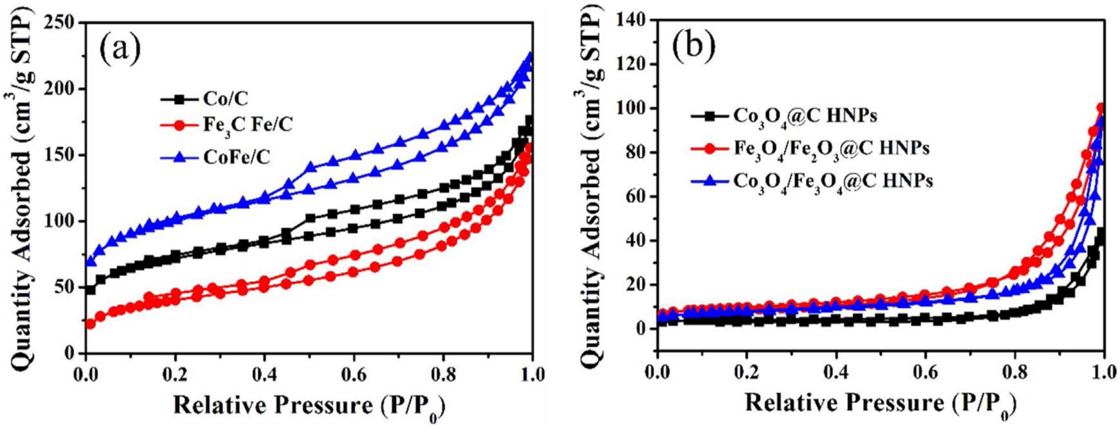

Fig. 3. N_2 adsorption-desorption isotherms of (a) MNPs/C, (b) MOHNPs@C.

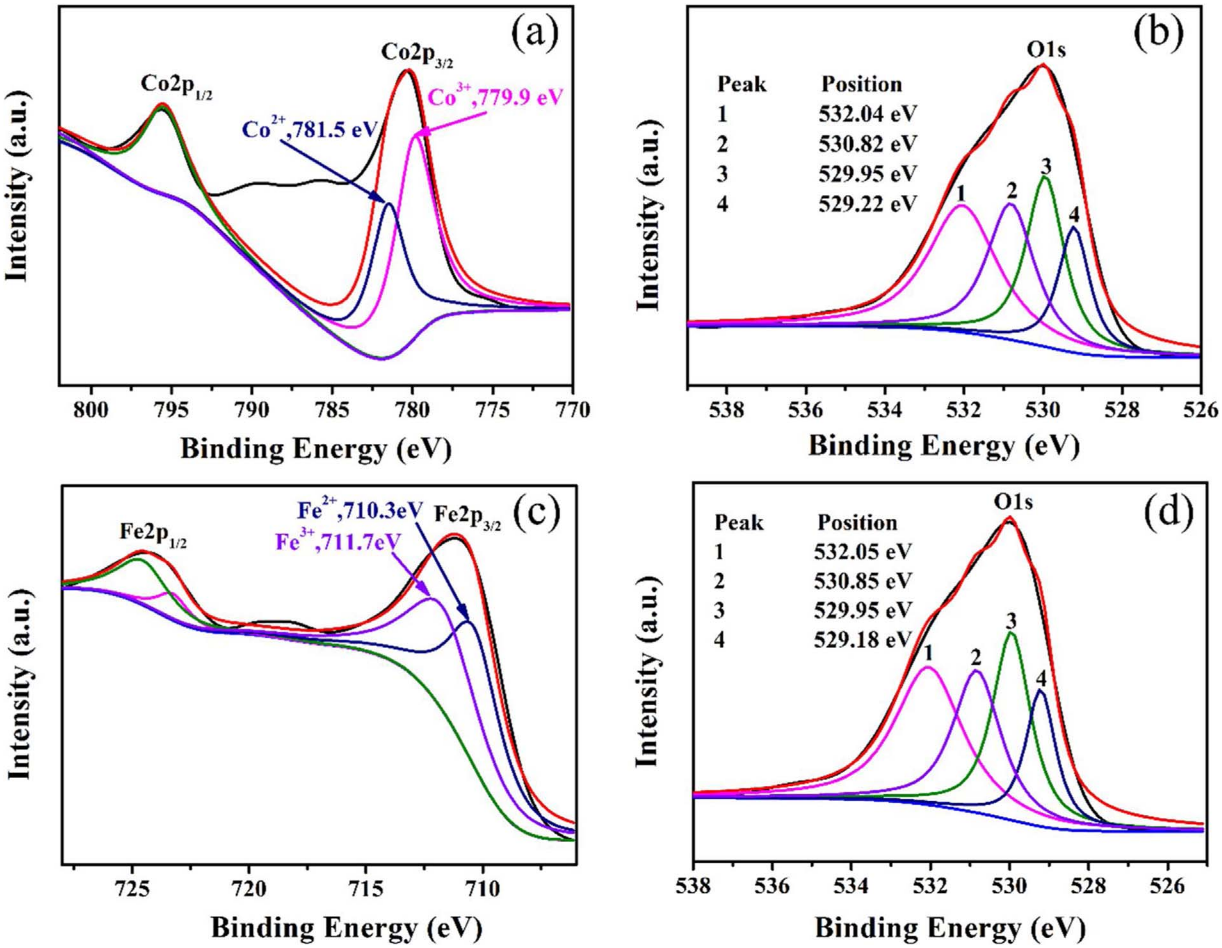

Fig. 4. (a) Co 2p, (b) O 1 s XPS pattern of Co_3O_4 (c) Fe 2p and (d) O1 s XPS pattern of Fe_3O_4.

reducibility [24,45], specific surface properties [18,46], and multi-component oxide crystal properties [17,47]. Moreover, and Co_3O_4 possess the higher catalytic activity compared to the Fe_3O_4/Fe_2O_3@C, which was attributed to that Fe_2O_3 is inactive in aerobic oxidation of alcohol [24].

Fig. 5 presents the catalytic results along with reaction time and reaction temperature for conversion of cinnamyl alcohol, product selectivity and yield, and turnover frequency (TOF). Fig. 5a and c show the catalytic performance of the Co_3O_4/Fe_3O_4@C along with the increase of reaction time, the conversion and yield are gradually raised and the selectivity is gradually reduce from 97% to 91%. And the TOF based conversion were moderate (ie., 45% and 18 h^{-1}). These results

Table 2
The catalytic activity of the different catalysts [a,b].

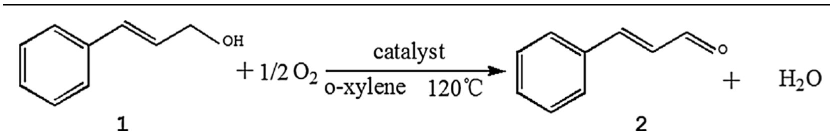

Entry	Catalyst	Conversion of 1 [%]	Selectivity of 2 [%]	Yield of 2 [%]
1	No catalyst	Trace		Trace
2	No catalyst(N_2)	No		No
3	Fe_3C/C	12	90	10.8
4	Co/C	10	92	9.2
5	CoFe/C	21	99	21
6	Fe_3O_4/Fe_2O_3@C	70	65	45.5
7	Co_3O_4@C	80	96	76
8[c]	Co_3O_4/Fe_3O_4@C	85	92	78
9	Co_3O_4/Fe_3O_4@C	96	93	~90
10[d]	Co_3O_4/Fe_3O_4@C	90	91	82
11	Co_3O_4/Fe_3O_4@C(N_2)	Trace		Trace

[a] The reaction was carried out using 20 mg of the catalyst, cinnamyl alcohol (4 mmol) and o-xylene (10 mL) in O_2 with 20 mL/min at 120 °C for 10 h.

[b] Determined by GC–MS measurement.

[c] Fe-Co mixed oxides with molar ratio of the range from 1:3.

[d] Fe-Co mixed oxides with molar ratio of the range from 3:1.

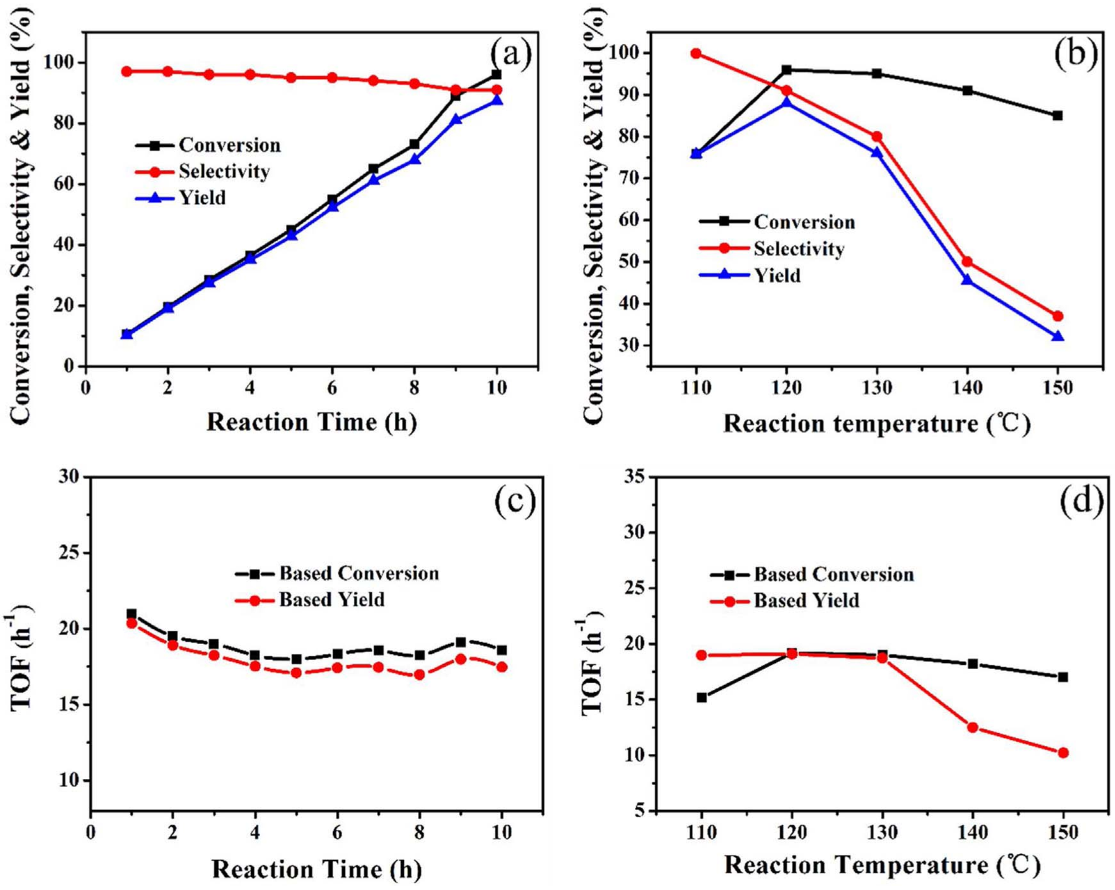

Fig. 5. Performance evaluation conversion, selectivity and yield, and TOF^a of $Co_3O_4/Fe_3O_4@C$ with (a) (c) reaction time and (b) (d) reaction temperature.
^{a}TOF based on the conversion of 1 h.

indicated that the decrease of selectivity and the TOF is due to byproducts (ie., acid). The sample was further tested at various reaction temperature, the catalytic results are shown in Fig. 4b and Fig. 5d. As the reaction temperature increased, the selectivity of cinnamyl aldehyde decreased from 98% to 37% and TOF based converion increased from 19 to 27.6 h^{-1}, but the based TOF based yield decreased from 19 to 10 h^{-1} and conversion decreased from 96 to 85% at 120 to150 °C. This phenomenon might not only be attributed to byproducts, but also be influenced for the surface activity or the catalysts particle aggregated by the higher temperature. And also, it is proved by the dynamic experiments (Fig. S5 and Table S2) with different surface adsorption rate constant.

To further obtain the substrate scope of the different selective alcohols oxidation reaction over the catalyst, various substrates including aliphatic and aromatic alcohols were carried out. The result was got in Table 3. It is clear that a range aliphatic alcohols (Entry 1–4) presented suit for the formation of the corresponding aldehydes or ketone, achieving moderate to good yields within 10 h. And the aliphatic alcohols (Entry 1–4) displayed higher activity than aromatic alcohols (Entry 5–9), this can be attributed the bimetallic oxide system, the coexistence of Fe and Cu in metal oxide leads to a modification of electronic and catalytic activity [48,49]. Moreover, the side reactions of the saturated and unsaturated alcohols are main the corresponding acid, and a spots of the unsaturated alcohols are the corresponding epoxide. Meanwhile, the para substituent of the electron-donating group (Entry 6) and the electron-withdraw group (Entry 7–9) have an obvious influence on the oxidation of alcohols and high electron density could improve the oxidative reaction of alcohol.

3.3. Kinetic study

The reaction kinetics of the oxidation of cinnamyl alcohol to cinnamyl aldehyde on the $Co_3O_4/Fe_3O_4@C$ catalyst with a series of cinnamyl alcohol concentrations were researched employing the initial reaction rate method. The result was presented the Supplementary Materials. The overall kinetics equation of the reaction can be defined as:

$$[\text{alcohol}] + \frac{1}{2}O_2 \overset{k}{\rightarrow} [\text{aldehyde}] + H_2O \tag{1}$$

Substituting $[O_2]$ as a constant, from earlier arguments, and considering reaction mechanism, the reaction process kinetics equations can be completed. The kinetic rate equation of absorption equilibrium was deduced with an equilibrium constant K_{ads} defined as:

$$K_{ads} = \frac{[\text{alcohol}]_{ads}}{[\text{alcohol}]_0\,[\text{cat}]} \tag{2}$$

and that the reaction mechanism for absorbed process of alcohol dehydrogenation refer to two sequential procedures according to [50]:

$$[\text{alcohol}]_{ads} \overset{k_1}{\rightarrow} [\text{alkoxy}]_{ads} \tag{3}$$

$$[\text{alkoxy}]_{ads} \overset{k_2}{\rightarrow} [\text{aldehyde}]_{ads} \tag{4}$$

the first dehydrogenation reaction rate constant of the alcohol is defined as k_1, and the second dehydrogenation reaction rate constant of the alcohol yielding to aldehyde is defined k_2. Nevertheless, in practice reaction process, these two procedures cannot be obtained and the degree of surface adsorption of substrate was considered [51].

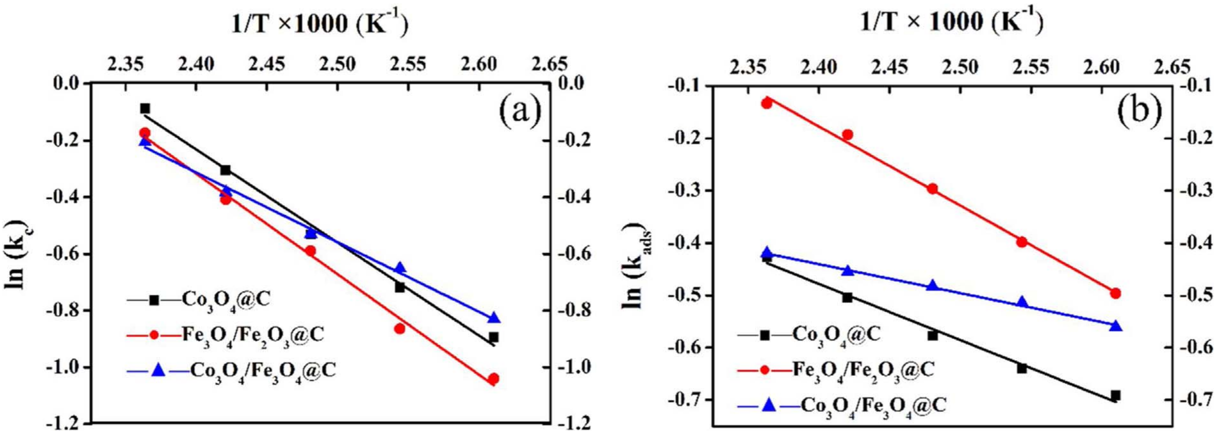

Fig. 6. Variation of the (a) E_{act} and (b) ΔQ for cinnamyl alcohol oxidation with alcohol on different catalysts.

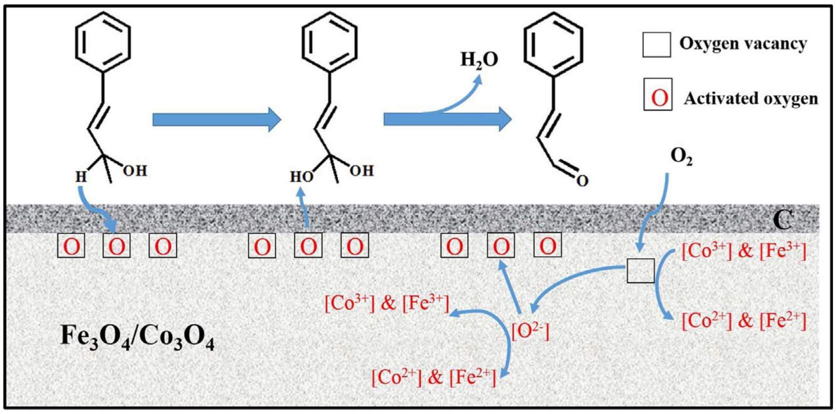

Fig. 7. The proposed mechanism for selective oxidation alcohol over the Co_3O_4/Fe_3O_4@C.

$$\theta = \frac{\lambda[\text{alcohol}]_0}{1+\lambda[\text{alcohol}]_0} \tag{5}$$

θ = ° of catalyst surface occupied by the substrate. λ = adsorption equilibrium constant.

The overall reaction kinetic equation can be transformed to [50–52]

$$r_0 = \frac{K_{ads}k_c[\text{cat}][\text{alcohol}]_0}{1+k_{ads}[\text{alcohol}]_0} \tag{6}$$

where k_c is a global kinetic constant

Which after linearization is converted into:

$$\frac{1}{r_0} = \frac{1}{K_{ads}k_c[\text{cat}][\text{alcohol}]_0} + \frac{1}{k_c[\text{cat}]} \tag{7}$$

Thus, via plotting the inverse of the initial reaction rate versus the inverse of the various initial concentration of alcohol, from the intercept and slope of the straight at the origin of the fitted equation, the values of k_c and k_{ads} can be obtained. The parallelism of experiment data to Eq. (7) in this work at different temperature is depicted in Fig. S4. Table S1 are summarized for the calculated kinetic and adsorption constants.

Activation energies E_{act} were calculated from the measured rate constants at different temperatures according to the Arrhenius equation:

$$k_c = Ae^{-E_{act}/RT} \tag{8}$$

$$\ln k_c = \ln A - \frac{E_{act}}{R}\left(\frac{1}{T}\right) \tag{9}$$

where E_{act} activation energy, R is the molar gas constant, T is the reaction temperature and A is the pre-exponential factor. Adsorption heat ΔQ of cinnamyl alcohol over the catalyst were obtained via the adsorption heat equation:

$$\ln K_{ads} = -\frac{\Delta Q}{R}\left(\frac{1}{T}\right) + C \tag{10}$$

Where ΔQ is the adsorption heat of the reaction, C is the constant, R is the molar gas constant and T is the reaction temperature.

Activation energy linearly and adsorption heat linearly are significantly different over the catalysts. It is indicated that the reaction underwent different reaction pathway over the catalysts (Fig. 6).

3.4. Proposed reaction mechanism

Based on the above results and discussion and the Co_3O_4/Fe_3O_4@C can presents an effective performance for selective oxidation of alcohol, an integrated reaction mechanism of selective oxidation of alcohol over the Co_3O_4/Fe_3O_4@C is proposed and shown in Fig. 7. To clarify the mechanism of aldehyde formation form the alcohol oxidation. The blank catalytic tests were conducted in N_2 and O_2 (Table 2 Entry 1 and 2). Under the condition, both the reaction condition do not exhibit catalytic activities, which imply the existence of a dehydrogenation mechanism in which aldehyde formation occurs in the absence of oxygen. The optimum catalyst carried out under N_2 was inactive, which indicated that the molecular is adsorbed and activated on the oxygen vacancy. Meanwhile, the oxygen adsorbed the oxygen vacancy will capture the transferred electrons and be activated, and the corresponding metal (Fe^{3+} and Co^{3+}) were reduced. The catalytic active center and the overall redox cycle of Fe_3O_4 and Co_3O_4 were completed. The activated oxygen attacks the alcohol to form C—O bond, and along with rapture of the C—H bond. The broken H atom transfers to the oxygen site to form O—H bond (C—OH group). Nevertheless, the two-OH is not stable and will be rearrangement to C=O and H_2O. The

Table 3
The yield of different substrates[a,b].

Entry	Substrate	Product	Reaction time (h)	Yield (%)
1	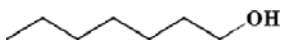	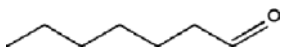	10	89.5
2	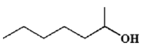	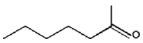	10	89.8
3	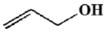	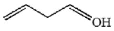	10	88.4
4	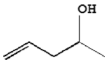	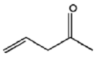	10	87.5
5	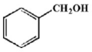	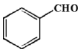	8	80.3
6	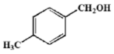	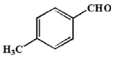	8	75.7
7	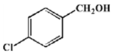	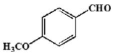	8	72.5
8	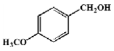	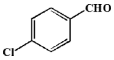	8	70.9
9	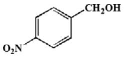	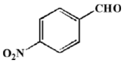	8	68.4

[a] The reaction was carried out using 20 mg of the catalyst, substrates (4 mmol) and o-xylene (10 mL) in O_2 with 20 mL/min at 120 °C.

[b] Determined by GC–MS measurement.

negative oxygen and positive alcohol react to obtain aldehyde and water.

It was proposed that the bimetal will inprove the transfer of electron and the cycle redox to improve the reaction activity (Table 3).

4. Conclusion

In summary, a functional bimetal oxide hollow nonacomposite ($Co_3O_4/Fe_3O_4@C$) has been designed and synthezied by a favorable method. $Co_3O_4/Fe_3O_4@C$ is a reasonable catalyst for aerobic oxidation carried out in heterogeneous reaction process with the liquid phase. The results demonstrated that the catalyst can be used as a substitute for the noble-metals-based catalyst to realize the alcohol oxidation process. the investigation of reaction process proved that the surface effect between metal oxide nanoparticle can present favorable catalytic activity for alcohol catalytic oxidation procedure. The dynamic experiment demonstrated that the active energy is different at diverse crystal structure of the catalyst. Hence, it provides a very-well feasible and economic pathway to apply to produce organic compounds in industrial manufacture.

Appendix A. Supplementary data

Supplementary data associated with this article can be found, in the online version, at http://dx.doi.org/10.1016/j.mcat.2018.01.028.

References

[1] T. Mallat, A. Baiker, Chem. Rev. 104 (2004) 3037–3058.
[2] Z. Guo, B. Liu, Q. Zhang, W. Deng, Y. Wang, Y. Yang, Chem. Soc. Rev. 43 (2014) 3480–3524.
[3] W.-H. Zhang, J.-J. Shen, J. Wu, X.-Y. Liang, J. Xu, P. Liu, B. Xue, Y.-X. Li, Mol. Catal. 443 (2017) 262–269.
[4] J. Piera, J.-E. Bäckvall, Angew. Chem. Int. Ed. 47 (2008) 3506–3523.
[5] J.U. Ahmad, P.J. Figiel, M.T. Räisänen, M. Leskelä, T. Repo, Appl. Catal. A: Gen. 371 (2009) 17–21.
[6] S. Zhu, Y. Cen, M. Yang, J. Guo, C. Chen, J. Wang, W. Fan, Appl. Catal. B: Environ. 211 (2017) 89–97.
[7] W. Hou, N.A. Dehm, R.W.J. Scott, J. Catal. 253 (2008) 22–27.
[8] N. Dimitratos, A. Villa, D. Wang, F. Porta, D. Su, L. Prati, J. Catal. 244 (2006) 113–121.
[9] J. Xu, J.-K. Shang, Y. Chen, Y. Wang, Y.-X. Li, Appl. Catal. A: Gen. 542 (2017) 380–388.
[10] C.-H. Liu, C.-Y. Lin, J.-L. Chen, K.-T. Lu, J.-F. Lee, J.-M. Chen, J. Catal. 350 (2017) 21–29.
[11] K. Kon, S.M.A. Hakim Siddiki, K.-i. Shimizu, J. Catal. 304 (2013) 63–71.
[12] H. Watanabe, S. Asano, S. -i. Fujita, H. Yoshida, M. Arai, ACS Catal. 5 (2015) 2886–2894.
[13] Y. Kuang, N.M. Islam, Y. Nabae, T. Hayakawa, M.-a. Kakimoto, Angew. Chem. Int. Ed. 49 (2010) 436–440.
[14] J. Zhu, J.L. Figueiredo, J.L. Faria, Catal. Commun. 9 (2008) 2395–2397.
[15] B. Karimi, S. Abedi, J.H. Clark, V. Budarin, Angew. Chem. Int. Ed. 37 (2006).
[16] S.E. Davis, M.S. Ide, R.J. Davis, Green Chem. 15 (2013) 17–45.
[17] J. Zhu, Y. Zhao, D. Tang, Z. Zhao, S.A.C. Carabineiro, J. Catal. 340 (2016) 41–48.
[18] G. Zhang, K.V. Vasudevan, B.L. Scott, S.K. Hanson, J. Am. Chem. Soc. 135 (2013) 8668–8681.
[19] S. Yang, L. Peng, P. Huang, X. Wang, Y. Sun, C. Cao, W. Song, Angew. Chem. Int. Ed. 55 (2016) 4016–4020.
[20] D. Sheet, T.K. Paine, Chem. Sci. 7 (2016) 5322–5331.
[21] R.V. Jagadeesh, H. Junge, M.-M. Pohl, J. Radnik, A. Brückner, M. Beller, J. Am. Chem. Soc. 135 (2013) 10776–10782.
[22] S.K. Hanson, R.T. Baker, J.C. Gordon, B.L. Scott, A.D. Sutton, D.L. Thorn, J. Am. Chem. Soc. 131 (2009) 428–429.
[23] Z. Shang, M. Sun, S. Chang, X. Che, X. Cao, L. Wang, Y. Guo, W. Zhan, Y. Guo, G. Lu, Appl. Catal. B: Environ. 209 (2017) 33–44.
[24] L. Geng, B. Zheng, X. Wang, W. Zhang, S. Wu, M. Jia, W. Yan, G. Liu, Chemcatchem 8 (2016) 805–811.
[25] S. Mandal, C. Santra, K.K. Bando, O.O. James, S. Maity, D. Mehta, B. Chowdhury, J. Mol. Catal. A: Chem. 378 (2013) 47–56.
[26] C. Miao, X.-X. Li, Y.-M. Lee, C. Xia, Y. Wang, W. Nam, W. Sun, Chem. Sci. 8 (2017) 7476–7482.
[27] F. Arena, B. Gumina, A.F. Lombardo, C. Espro, A. Patti, L. Spadaro, L. Spiccia, Appl. Catal. B: Environ. 162 (2015) 260–267.
[28] Y. Du, Q. Wang, X. Liang, P. Yang, Y. He, J. Feng, D. Li, Catal. Sci. Technol. 7 (2017) 4361–4365.
[29] Y. Chen, H. Zheng, Z. Guo, C. Zhou, C. Wang, A. Borgna, Y. Yang, J. Catal. 283 (2011) 34–44.
[30] K. Sarmah, J. Pal, T.K. Maji, S. Pratihar, ACS Sustain. Chem. Eng. 5 (2017) 11504–11515.
[31] K. Jirátová, F. Kovanda, J. Balabánová, P. Kšírová, Catal. Today (2017).
[32] L. Pi, N. Yang, W. Han, W. Xiao, D. Wang, Y. Xiong, M. Zhou, H. Hou, X. Mao, Chem. Eng. J. 334 (2017) 1297–1308.
[33] H. Lan, X. Xiao, S. Yuan, B. Zhang, G. Zhou, Y. Jiang, Catal. Lett. 147 (2017) 2187–2199.
[34] A. Dhakshinamoorthy, M. Alvaro, H. Garcia, ACS Catal. 1 (2011) 836–840.
[35] Y. Brik, M. Kacimi, M. Ziyad, F. Bozon-Verduraz, J. Catal. 202 (2001) 118–128.
[36] X. Xie, Y. Li, Z.-Q. Liu, M. Haruta, W. Shen, Nature 458 (2009) 746–749.
[37] J. Wei, Q. Ge, R. Yao, Z. Wen, C. Fang, L. Guo, H. Xu, J. Sun, Nat. Commun. 8 (2017) 15174.
[38] J. Zhu, K. Kailasam, A. Fischer, A. Thomas, ACS Catal. 1 (2011) 342–347.
[39] T. Zeng, M. Yu, H. Zhang, Z. He, J. Chen, S. Song, Catal. Sci. Technol. 7 (2016).
[40] Y. Yang, X. Fan, G. Casillas, Z. Peng, G. Ruan, G. Wang, M.J. Yacaman, J.M. Tour, Acs Nano 8 (2014) 3939–3946.
[41] L. Geng, M. Zhang, W. Zhang, M. Jia, W. Yan, G. Liu, Catal. Sci. Technol. 5 (2015) 3097–3102.
[42] J. Jansson, A.E.C. Palmqvist, E. Fridell, M. Skoglundh, L. Österlund, P. Thormählen, V. Langer, J. Catal. 211 (2002) 387–397.
[43] J.-l. Tu, M.-y. Ding, Q. Zhang, Y.-l. Zhang, C.-g. Wang, T.-j. Wang, L.-l. Ma, X.-j. Li, ChemCatChem 7 (2015) 2323–2327.
[44] J. Lu, X. Jiao, D. Chen, W. Li, J. Phys. Chem. C 113 (2009) 4012–4017.
[45] F.A. Westerhaus, R.V. Jagadeesh, G. Wienhöfer, M.-M. Pohl, J. Radnik, A.-E. Surkus, J. Rabeah, K. Junge, H. Junge, M. Nielsen, A. Brückner, M. Beller, Nat. Chem. 5 (2013) 537–543.
[46] J. Zhu, S.A.C. Carabineiro, D. Shan, J.L. Faria, Y. Zhu, J.L. Figueiredo, J. Catal. 274 (2010) 207–214.
[47] K.-i. Shimizu, K. Kon, M. Seto, K. Shimura, H. Yamazaki, J.N. Kondo, Green Chem. 15 (2013) 418–424.
[48] Y. Li, Y. Gao, C. Yang, Chem. Commun. 51 (2015) 7721–7724.
[49] W. Gao, S. Li, H. Huo, F. Li, Y. Yang, X. Li, X. Wang, Y. Tang, R. Li, Mol. Catal. 439 (2017) 108–117.
[50] M. Boronat, A. Corma, F. Illas, J. Radilla, T. Ródenas, M.J. Sabater, J. Catal. 278 (2011) 50–58.
[51] V.D. Makwana, Y.-C. Son, A.R. Howell, S.L. Suib, J. Catal. 210 (2002) 46–52.
[52] X. Huang, H. Li, W.-D. Xiao, D. Chen, Chem. Eng. J. 299 (2016) 263–275.